ISSN (Print) 1226-1750
ISSN (Online) 2233-6656
Journal of Magnetics 26(3), 243-248 (2021) https://doi.org/10.4283/JMAG.2021.26.3.243

Large Magnetization in Self-assembled 1D Chain-like α-Fe_2O_3 Nanostructures Synthesized by a Facile Solvothermal Method

Minji Gu[1], Shanigaram Mallesh[1], and Ki Hyeon Kim*

Department of Physics, Yeungnam University, Gyeongsan 38541, Republic of Korea
[1]Both Authors Contributed Equally

(Received 2 July 2021, Received in final form 25 August 2021, Accepted 25 August 2021)

The 1D chain-like α-Fe_2O_3 nanostructures were synthesized using a facile solvothermal method followed by subsequent annealing in air at 450 °C for two hours. We have investigated the microstructure and magnetic properties of the samples in detail. Field emission scanning electron microscopy revealed the formation of 1D chain-like morphology of α-Fe_2O_3 nanostructures. The presence of the pure hematite phase in all samples was confirmed by X-ray diffraction (XRD). Further, results obtained from Raman and FT-IR spectra are consistent with XRD outcomes. The magnetic studies (M-H curves) of samples exhibited a wide range of properties. The S_1 and S_5 samples exhibit large coercivity (H_C) values of 878 Oe and 1092 Oe, respectively. Interestingly, large magnetization 15 emu/g and lowest H_C (= 56 Oe) were observed for sample S_2 compared to all other samples. The unusual magnetic properties of the samples are due to morphology (shape, size, and self-assembled 1D orientation of particles), surface spin disorder, and (surface/interface) anisotropy of the nanoparticles.

Keywords : solvothermal, self-assembly, 1D nano chains, α-Fe_2O_3, nanostructures, magnetization, coercivity

1. Introduction

Recently, the micro/nanostructures with controllable shape, size, and composition have vital interest due to their intriguing chemical, optical, and magnetic properties [1]. Hematite (α-Fe_2O_3) is an n-type semiconductor (E_g = 2.1 eV), which is the most stable iron oxide under ambient conditions. It is a fascinating multifunctional material due to its extraordinary resistance to corrosion, low processing cost, non-toxic, and environmentally friendly properties. Therefore, α-Fe_2O_3 is worthwhile in various potential applications such as sensors, supercapacitors, lithium-ion batteries, and water splitting [2-5]. The bulk α-Fe_2O_3 is a well-known antiferromagnetic (Neel temperature (T_N) = 950 K) with a Dzyaloshinskii-Moriya interaction it undergoes a Morin transition T_M (T_M = 263 K) [6]. Furthermore, α-Fe_2O_3 nanoparticles also shown a superparamagnetic nature when the particle size decreased below 20 nm. The size of the α-Fe_2O_3 nanoparticles strongly influences both superparamagnetic blocking temperature and Morin transition temperature [7, 8]. Several authors have prepared self-assembled α-Fe_2O_3 superstructures with different morphologies, and they observed that the morphologies significantly affect physical/chemical properties [1, 3, 9]. Recently, self-orientation techniques have been extensively employed due to their facile synthesis and low cost. The inorganic building blocks such as nanoparticles, rods, sheets, discs, spheres, and polyhedrons were self-assembled in particular directions to form periodically ordered superstructures [3, 9]. As anticipated, these α-Fe_2O_3 superstructures exhibit morphology-dependent physical/chemical properties. Therefore, the synthesis of multifunctional self-assembled α-Fe_2O_3 superstructures has become an increasingly attractive topic [1, 9, 10]. Sun *et al.* have synthesized the self-assembled α-Fe_2O_3 nanoplates aligned into one-dimensional (1D) columnar superstructures by hydrothermal method. The α-Fe_2O_3 1D columnar superstructures revealed high ethanol and formaldehyde sensitivity [11]. Chen *et al.* have shown nanostructures assembled from large α-Fe_2O_3 nanoparticles obtained from the hydrothermal process. Furthermore, they have observed that the 2D structures are formed into 3D superstructures by dipole-dipole interactions [12]. Muruganandham *et al.* prepared porous rods and chain-like α-Fe_2O_3 structures using oxalate in thermal decomposition method and investigated

*Corresponding author: Tel: +82-53-810-2334
Fax: +82-53-810-4616, e-mail: kee1@ynu.ac.kr

the electrochemical properties [13]. Amutha *et al.* prepared the crystallization-induced wormlike hierarchical self-assembly porous hematite, which shown arsenic removal capacity [14]. Komal *et al.* designed the chain-like α-Fe_2O_3 structures using alkyl groups. They have observed that the morphological, magnetic, and photocatalytic properties of the chain-like α-Fe_2O_3 structures depend on the alkyl chain groups [15]. Therefore, developing facile and reliable procedures to grow the 1D chain-like α-Fe_2O_3 nanostructures with well-ordered morphologies is interesting for several potential applications but remains a significant challenge.

Herein, we have fabricated 1D chain-like α-Fe_2O_3 nanostructures via a simple solvothermal method without using any templates. This work provides controlling 1D chain-like α-Fe_2O_3 nanostructures. Moreover, the prepared self-assembled 1D chain-like α-Fe_2O_3 nanostructures can be ideal for systematically studying their shape/size-dependent catalytic, optic, and magnetic properties.

2. Experimental Details

2.1. Chemical

The following chemicals of iron (III) nitrate ($Fe(NO_2)_3 \cdot 9H_2O$, 98 %, Sigma Aldrich), *N,N*-dimethyl formaldehyde (DMF, Sigma Aldrich, 99 %) ethylene glycol, (EG, $C_2H_6O_2$, Sigma Aldrich 99.8 %), ethanol (C_2H_5OH) and deionized (DI) used in this experiment. These chemicals are used as received without any purification.

2.2. Synthesis

To synthesize the self-assembled 1D chain-like α-Fe_2O_3 nanostructures, 0.808 g of $Fe(NO_2)_3 \cdot 9H_2O$ dissolved in 40 ml of EG and 20 ml of DMF solution under magnetic stirring. Then the solution shifted to a Teflon-lined stainless steel autoclave (100 ml capacity) placed in an oven and reacted at 180 °C for 22 h. Various samples have been prepared by changing the experimental conditions, as shown in Table 1. The as-synthesized precursors were annealed at 450 °C in air to investigate the microstructure and magnetic properties of the samples.

The field emission scanning electron microscopy (FESEM, Hitachi, S-4800) is used to analyze the morphology of samples. The structural phase formation is characterized using X-ray diffraction (XRD) using PANalytical (X'pert PRO, CuKα (λ = 1.54059 Å)). The vibrational properties of the samples were examined at room temperature using Raman spectra (Horiba JOBIN YVON, Lab RAM HR) and Fourier transform infrared (FT-IR) spectrophotometer (Perkin Elmer Co. LTD). The isothermal magnetization was measured using a vibrating sample magnetometer (VSM).

3. Results and Discussions

Figure 1 shows the FESEM images of α-Fe_2O_3 nanostructures obtained under different processing conditions. The sample S_1 displays the self-assembled nanoparticles with an average diameter of particles is 45 nm. These nanoparticles were grown into self-assembled 1D chain-like α-Fe_2O_3 superstructures with a few 100 nm lengths. Further, these 1D orientated superstructures were self-assembled, as shown in Fig. 1(a_1-a_3) for sample S_1. Additionally, we have studied the influence of changing conditions on 1D self-assembled α-Fe_2O_3 superstructures. Fig. 1(b_1-b_3) sample S_2 exhibits highly uniform self-assembly of 1D chain-like α-Fe_2O_3 superstructures compared to all other samples. The average diameter of particles is 45 nm, nearly identical with sample S1, but these nanoparticles attached end to end in 1D chain-like orientated superstructures with an increased length up to a few μm. Fig. 1(c_1-c_3) displays the self-assembled chain-like α-Fe_2O_3 superstructures for sample S_3, which is also similar to sample S_2, but the average particle size (42 nm) and length of 1D chain-like α-Fe_2O_3 orientated superstructures decreased compared to S_2. Further, 1D orientated α-Fe_2O_3 superstructures particle size (34 nm) and length are significantly reduced for sample S_4, as shown in Fig. 1(d_1-d_3). The self-assembled 1D chain-like α-Fe_2O_3 orientated superstructures are less prominent in samples

Table 1. The variation of experimental conditions used to grow the self-assembled 1D chain-like α-Fe_2O_3 nanostructures.

Samples	Solvents				Reaction temperature (°C)	Reaction time (hours)
	EG (ml)	DMF (ml)	DI water (ml)	Glycerol (ml)		
S1	50	10			180	22
S2	40	20			180	22
S3	40	20	1		180	22
S4	40	20	5		180	22
S5	40	20		1	180	22
S6	40	20		5	180	22

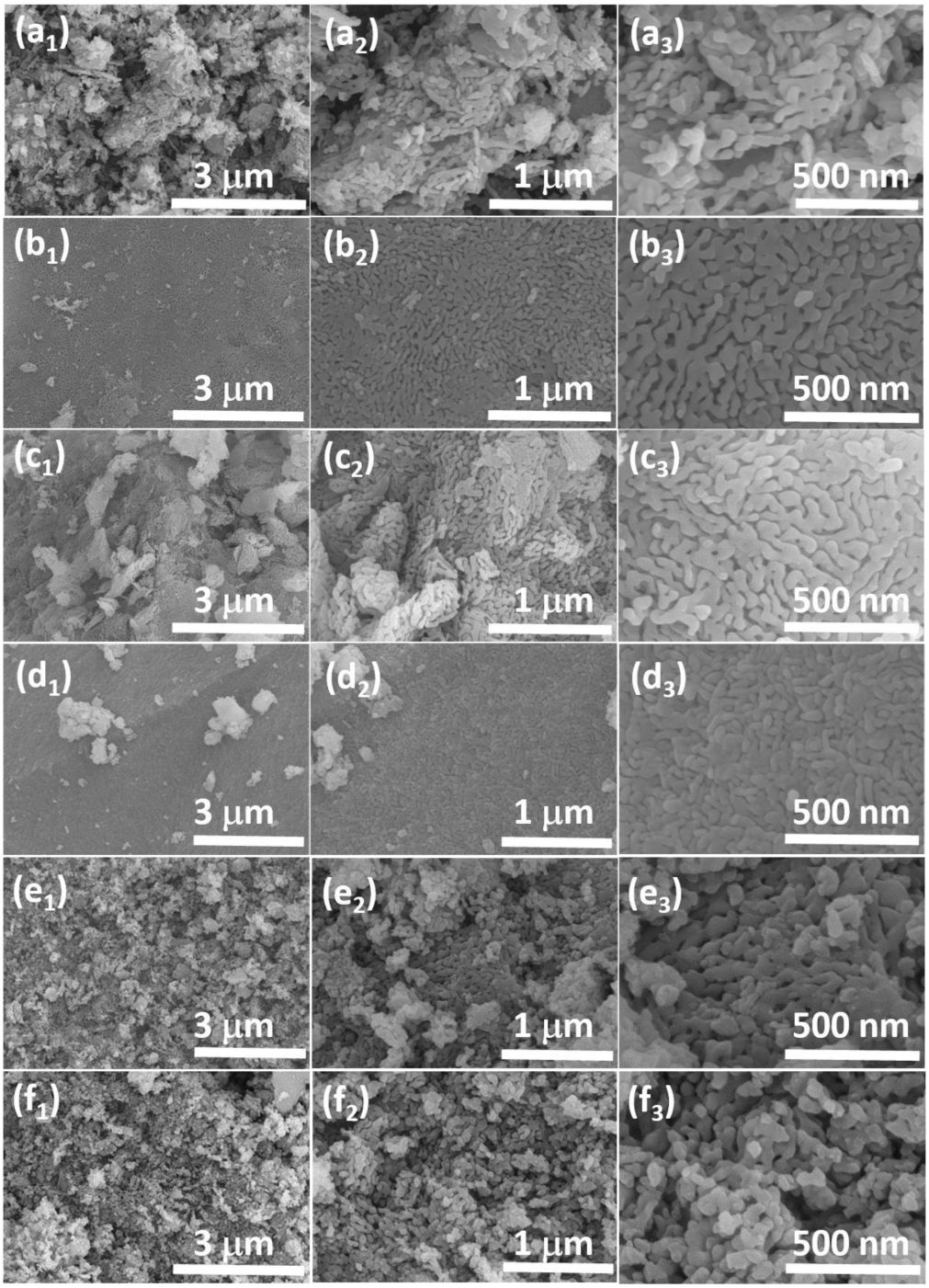

Fig. 1. FESEM images of self-assembled 1D chain-like α-Fe_2O_3 nanostructures (a_1-a_3) S_1, (b_1-b_3) S_2, (c_1-c_3) S_3, (d_1-d_3) S_4, (e_1-e_3) S_5, and (f_1-f_3) S_6, samples, respectively.

S_5 and S_6, as revealed in Fig. 1(e_1-e_3) and Fig. 1(f_1-f_3).

Based on the above experimental results, the possible mechanism for the 1D orientated superstructures is proposed, as demonstrated in Fig. 2. The Fe^{3+} ions initiated nucleation in EG and DMF solvent. These nuclei aggregate together and grow the nanoparticles, whose size increases with the reaction time. Further, these nanoparticles were assembled into 1D orientated α-Fe_2O_3 superstructures. Finally, self-assembled 1D chain-like α-Fe_2O_3 superstructures formed as a result of continuous self-assembled growth of nanoparticles.

Figure 3 shows the XRD patterns of α-Fe_2O_3 nanostructures obtained under various processing conditions. All the samples exhibited pure hematite phase (α-Fe_2O_3)

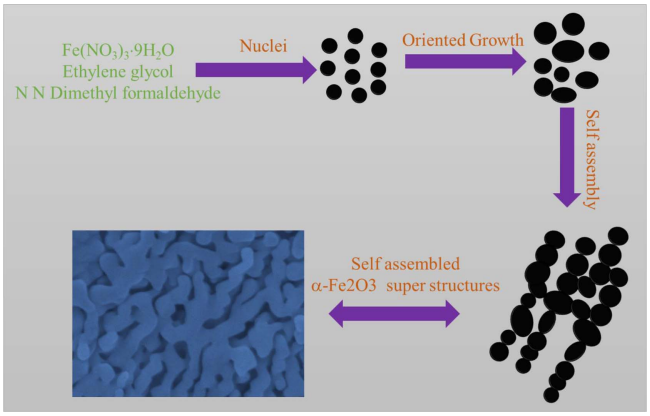

Fig. 2. (Color online) Schematic illustration for the formation of self-assembled 1D chain-like α-Fe_2O_3 nanostructures.

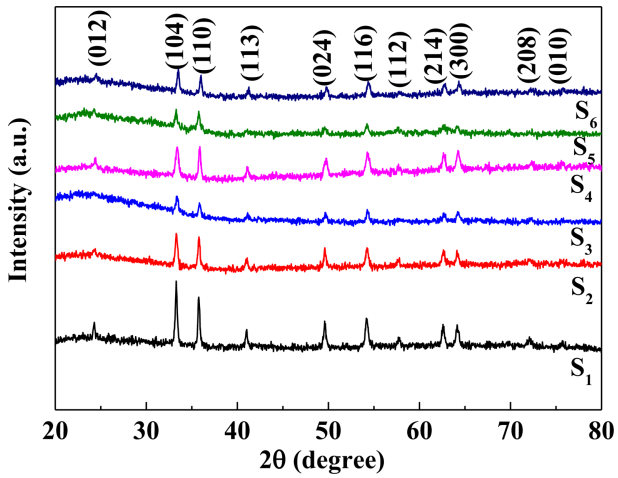

Fig. 3. (Color online) XRD patterns of self-assembled 1D chain-like α-Fe_2O_3 nanostructures obtained under different conditions.

deprived of any noticeable quantity of impurity phases. The perceived XRD patterns of all samples agree well with the rhombohedral crystal structure [space group: R-3c] of α-Fe_2O_3 (JCPDS file no. 33-0664). The sharpness of the observed peaks manifests the good crystallinity of the α-Fe_2O_3 samples. We used the Scherrer formula to evaluate the average crystallite sizes of the samples for the six high-intensity peaks, and the found values are presented in Table 2. The estimated crystallite size is 42 nm for S_1 sample, which decreases to 40 nm for S_2; that is when EG decreased to 40 ml from 50 ml, and DMF has increased from 10 ml to 20 ml (S2). Further, with the addition of DI water 1 ml and 5 ml, the crystallite size decreased to 36.6 and 33.4 nm for samples S_3 and S_4, respectively. Similarly, the crystallite size is reduced when glycerol is added to the above solution, as shown in Table 2. The presence of mixed solvents, their specific absorption of organic groups, and the high boiling temperature of the solvents can control the size and morphology of the α-Fe_2O_3 nanostructures [1-3]. The lattice strain values of samples presented in Table 2 are in agreement with the nano crystallinity of samples.

Raman spectroscopy is used to study the vibrational properties and to confirm the structural phase formations further. The Raman spectra of α-Fe_2O_3 nanostructures show the occurrence of a pure phase of α-Fe_2O_3 modes

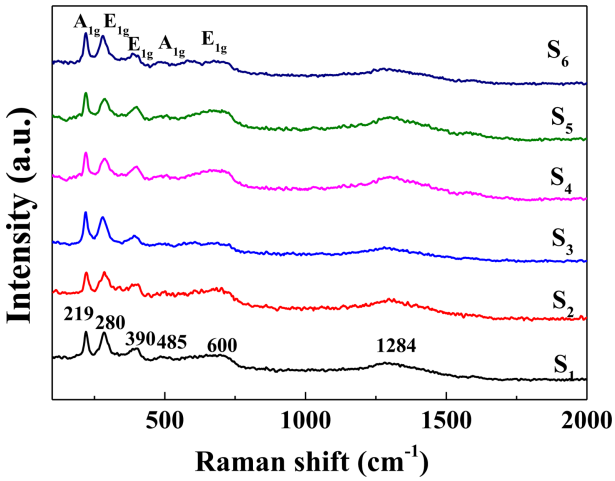

Fig. 4. (Color online) Raman spectra of self-assembled 1D chain-like α-Fe_2O_3 nanostructures obtained under different conditions.

Table 2. The Structural and magnetic parameters of self-assembled 1D chain-like α-Fe_2O_3 nanostructures. The t, h, and D are crystallite size, lattice strain, and particle size.

Samples	t (nm)	η	D (nm)	M (emu/g)	M_R (emu/g)	H_C (Oe)
S1	42.2	0.25	45	0.89	0.22	878
S2	40.5	0.24	45	15.88	1.75	56
S3	36.6	0.31	42	3.2	0.23	74
S4	33.4	0.32	34	0.33	0.14	398
S5	38.5	0.28	47	0.87	0.22	782
S6	36.8	0.28	45	0.84	0.23	1092

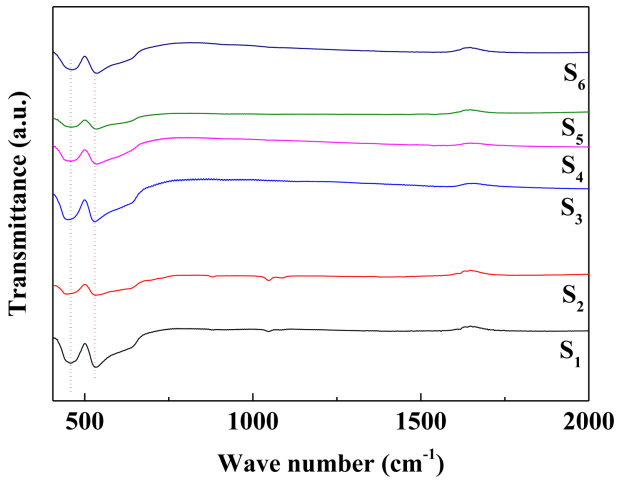

Fig. 5. (Color online) FT-IR of self-assembled 1D chain-like α-Fe_2O_3 nanostructures obtained under different conditions.

nearby 219 cm^{-1}, 280 cm^{-1}, 390 cm^{-1}, 485 cm^{-1}, 609 cm^{-1}, 690 cm^{-1}, and 1284 cm^{-1}, as shown in Fig. 4. The Raman modes observed at 219 and 485 cm^{-1} are attributed to the A_{1g} associated with the motion of Fe cations along the c axis of the unit cell. The other modes, observed around 280 cm^{-1}, 390 cm^{-1}, and 609 cm^{-1}, are assigned to the E_g modes due to the symmetric breathing of the O atoms relative to each cation perpendicular to the crystallographic c axis of the unit cell [16]. In addition, the Raman mode E_g was observed at 690 cm^{-1} owing to the order-disorder related to surface effects or the existence of small α-Fe_2O_3 nanocrystals the Raman mode observed at 1284 cm^{-1} has been allotted to the two magnon scattering, which arises from the antiparallel adjacent spins [16, 17]. Fig. 5 demonstrates the FT-IR spectra α-Fe_2O_3 samples display two noticeable vibrational bands around 455 cm^{-1} correspondings to the bending vibration of O-Fe-O and 534 cm^{-1} attributed stretching of Fe-O [16]. No other peaks corresponding to other phases were observed indicate that the samples formed pure α-Fe_2O_3. Therefore, Raman and FT-IR spectra advance to confirm the pure hematite phase, which agrees with XRD results.

Figure 6 describes the magnetic field (± 15 kOe) dependent magnetization (M) of α-Fe_2O_3 nanostructures. Overall, samples exhibit wide variation in magnetic properties. From the M-H curves, the attained values of M (taken at 15 kOe), remnant magnetization (M_R), and coercivity (H_C) are presented in Table 2. Except for sample S_2, no saturation magnetization was attained within the applied magnetic field for all samples. These samples exhibit weak ferromagnetic performance, which arises from the canted antiferromagnetic nature. These results are in agreement with earlier reports on α-Fe_2O_3 nanostructures [17-19]. Fig. 6 S_1 sample shows the M ~ 0.89 emu/g and M_R ~ 0.25 emu/g and H_C (878 Oe). Sample S_2 exhibits large magnetization 15.8 emu/g with the lowest coercivity (56 Oe). This value is noticeably more significant than the different samples from our work and other reports on α-Fe_2O_3 nanostructures, which typically exhibit below 1 emu/g [17-19]. In contrast, Manukyan *et al.* also observed high M (21 emu/g) in ultrasmall superparamagnetic nanoparticles synthesized by template-assisted auto combustion method [20]. This unusual magnetization in α-Fe_2O_3 nanoparticles is attributed to the surface spin structure. The M-H curve of sample S_3 exhibits similar to sample S_2, but M is decreased to 3.2 emu/g could be due to a change in surface spin structure. Noticeably, the lowest value of M 0.33 emu/g was observed for sample S_4. Further samples S_5 and S_6 exhibit very similar behavior with values of M are 0.87 and 0.84 emu/g, respectively. The value of H_C is 878 Oe observed for sample S_1, which significantly reduced to 56 Oe for sample S_2. Then the values of H_C systematically increased from sample S_2 to S_6. The highest value of H_C is 1092 Oe observed for sample S_6. The high values of H_C from previous reports on α-Fe_2O_3 nanostructures revealed several

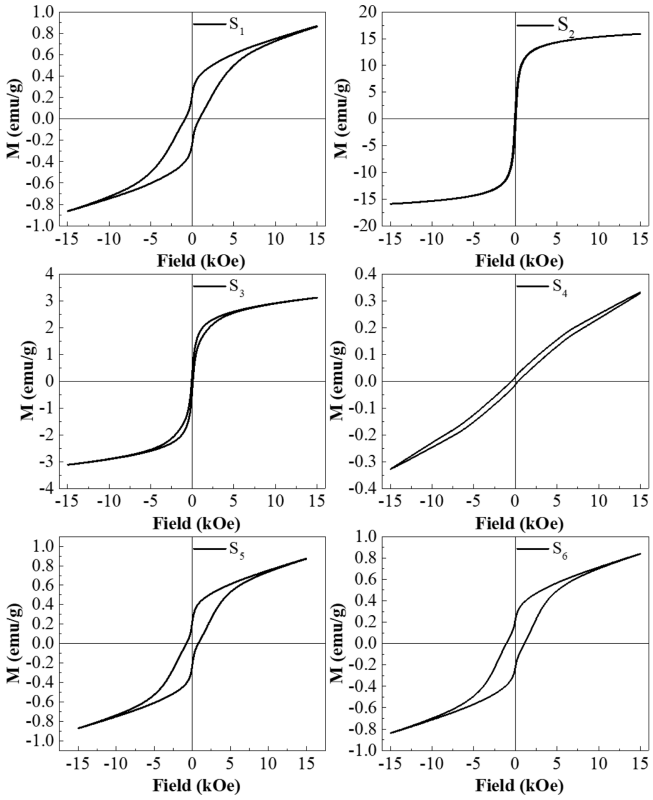

Fig. 6. M-H curves measured at room temperature for self-assembled 1D chain-like α-Fe_2O_3 nanostructures obtained under different conditions.

aspects [6, 17-19]. The large value of H_C originating from morphology, surface spin disorder, the orientation of nanoparticles, anisotropy, and inter/intra particles interactions of nanoparticles in the nanostructures. Interestingly, S_1, S_5, and S_6 exhibit a kink behavior in low fields of M-H curves. Similar behavior is witnessed in earlier reports on α-Fe_2O_3 nanostructures [21-23]. The kink in can be observed because the spin-flip reverses the magnetic sublattice, which is antiparallel to the magnetic field [24]. From the simulations, they have shown that the kink behavior in two single domains and a superparamagnetic grain system. The hard and soft magnetic phases combination leads to a jump in the hysteresis loop near-zero magnetic fields. Furthermore, two-phase magnetic systems (e-Fe_2O_3 + α-Fe_2O_3), with different coercivities, display a kink in hysteresis loops [25]. Therefore, surface spin structure, the heterogeneous size distribution of the nanostructures, and the presence of hard/soft magnetic phases can be the reason for the existence of kink in the hysteresis loop. The developed uniform 1D chain-like α-Fe_2O_3 nanostructures can be used for catalytic, optics, and magnetism applications.

4. Conclusions

The self-assembled 1D chain-like α-Fe_2O_3 nanostructures were successfully synthesized by a facile solvothermal method. FESEM analysis confirmed the formation of 1D chain-like morphology of α-Fe_2O_3 nanostructures. The formation of the hematite crystal structure has been confirmed from the XRD study. Further, phase formation is supported by Raman and FT-IR studies. Higher Hc, 878 Oe, and 1092 Oe, respectively, were observed for S_1 and S_5 samples. Moreover, large magnetization 15 emu/g and lowest Hc (= 56 Oe) were observed for sample S_2. The variations in magnetic properties originated from the morphology, surface spin disorder, surface/interface anisotropy of self-assembled nanoparticles.

Acknowledgment

This research was supported by Creative Materials Discovery Program through the National Research Foundation of Korea (NRF) funded by Ministry of Science and ICT (2020M3D1A2080950).

References

[1] X. Hu and J. C. Yu, Adv. Funct. Mater. **18**, 880 (2008).
[2] Z. Sun, H. Yuan, Z. Liu, B. Han, and X. Zhang, Adv. Mater. **17**, 2993 (2005).
[3] S. Yu, V.-H. Ng, F. Wang, Z. Xiao, C. Li, L. B. Kong, W. Que, and K. Zhou, J. Mater. Chem. A **6**, 9332 (2018).
[4] Y. Yang, Y. Liu, K. Pu, X. Chen, H. Tian, M. Gao, M. Zhu, and H. Pan, Adv. Funct. Mater. **27**, 1605011 (2017).
[5] Y. Zhang, Y. Huang, S.-S. Zhu, Y.-Y. Liu, X. Zhang, J.-J. Wang, and A. Braun, Small **17**, 2100320 (2021).
[6] H. Jani *et al.* Nature. Commun. **12**, 1668 (2021).
[7] M. Tadic, N. Citakovic, M. Panjan, Z. Stojanovic, D. Markovic, and V. Spasojevic, J. Alloy. Compd. **509**, 7639 (2011).
[8] M. Tadic, M. Panjan, V. Damnjanovic, and I. Milosevic, Appl. Surf. Sci. **320**, 183 (2014).
[9] J. Lian, X. Duan, J. Ma, P. Peng, T. Kim, and W. Zheng, ACS Nano **3**, 3749 (2009).
[10] J.-S. Xu and Y. J. Zhu, CrystEngComm **13**, 5162 (2011).
[11] J. Sun, K.-L. Wu, X.-Z. Li, C. Dong, X.-W. Wei, X.-W. Wang, B. Zhang, Z.-X. Zhang, and J.-R. Huang, CrystEngComm **16**, 6873 (2014).
[12] J. S. Chen, T. Zhu, C. M. Li, and J. W. Lou, Angew. Chem. Int. Ed. **50**, 650 (2011).
[13] M. Muruganandham, R. Amutha, M. Sathish, T. S. Singh, R.-S. Suri, and M. Sillanpaa, J. Phys. Chem. C **115**, 18164 (2011).
[14] R. Amutha, M. Muruganandham, M. Sathish, S. Akilandeswari, R.-S. Suri, E. Repo, and M. Sillanpaa, J. Phys. Chem. C **115**, 6367 (2011).
[15] Komal, H. Kaur, M. Kainth, S. S. Meena, and T. S. Kang, RSC Adv. **9**, 41803 (2019).
[16] H. Zhu, J. Deng, J. Chen, R. Yu, and X. Xing, J. Mater. Chem. A **2**, 3008 (2014).
[17] L. Kopanja, I. Milosevic, M. Panjan, V. Damnjanovic, and M. Tadic, Appl. Surf. Sci. **362**, 380 (2016).
[18] X. Zhang, Y. Chen, H. Liu, Y. Wei, and W. Wei, J. Alloy. Compd. **555**, 74 (2013).
[19] J. Liu, H. Yang, and X. Xue, CrystEngComm **21**, 1097 (2019).
[20] K.V. Manukyan, Y.-S. Chen, S. Rouvimov, P. Li, X. Li, S. Dong, X. Liu, J. K. Furdyna, A. Orlov, G. H. Bernstein, W. Porod, S. Roslyakov, and A. S. Mukasyan, J. Phys. Chem. C **118**, 16264 (2014).
[21] S. Mallesh, D. Narsimulu, and K. H. Kim, Phys. Lett. A **384**, 126038 (2020).
[22] R. Kant, D. Kumar, and V. Dutta, RSC Adv. **5**, 52945 (2015).
[23] Y. Yang, J. B. Yi, X. L. Huang, and J. Ding, IEEE Trans. Magn. **47**, 3340 (2011).
[24] L. Tauxe, T. A. T. Mullender, and T. Pick, J. Geophys. Res. Solid Earth **101**, 571 (1996).
[25] V. N. Nikolic, V. Spasojevic, M. Panjan, L. Kopanja, A. Mrakovic, and M. Tadic, Ceram. Int. **43**, 7497 (2017).